Free Vibration Analysis of In-plane Frame Structures by the Transfer Influence Coefficient Method

Inoue, Takumi
Department of Intelligent Machinery and Systems, Kyushu University : Associate Professor

Sueoka, Atsuo
Department of Intelligent Machinery and Systems, Kyushu University : Professor

出版情報：九州大学工学紀要. 67 (2), pp.33-51, 2007-06. 九州大学大学院工学研究院
バージョン：
権利関係：

Memoirs of the Faculty of Engineering, Kyushu University, Vol.67, No.2, June 2007

Free Vibration Analysis of In-plane Frame Structures by the Transfer Influence Coefficient Method

by

Takumi INOUE* and Atsuo SUEOKA**

(Received March 18, 2007)

Abstract

The Transfer Influence Coefficient Method is an advantageous device used to analyze a dynamic response of a multi degree of freedom system. The Transfer Influence Coefficient Method conquered some disadvantages of the Transfer Matrix Method and has some advantages in computational accuracy and speed. However, this method was not available to treat truss and rahmen structures since the algorithm was incapable of branches and links to form a closed loop in truss and rahmen structures. In this paper, a new algorithm of the Transfer Influence Coefficient Method for an in-plane free vibration analysis of frame structures with closed loops is presented. The new algorithm still retains the advantages of the original algorithm on the computational accuracy and speed. The advantages are demonstrated through a free vibration analysis, compared with a conventional routine.

Keywords: Computational method, Truss structure, Pin joint, Free vibration, Transfer Matrix Method, Transfer Influence Coefficient Method

1. Introduction

A large scale structure such as a skyscraper or a long spanning bridge is sensitive to strong winds and earthquakes. A dynamic response analysis of the structure is indispensable to help prevent destruction and to aid in the inquiry of accidents. Since the structure has a large degree of freedom, a great deal of computational cost is still required even if a currently developed computer is utilized. In order to overcome this difficulty, some devices to reduce the degree of freedom were proposed. The most popular method seemed to be the modal analysis[1)-3)]. Several characteristic modes corresponding to low natural frequencies were usually employed to the modal analysis. The condensation method[4)] is an alternate and is often implemented. Some devices to improve the static condensation method were proposed[5)-7)], and showed a better performance than the simple static method. In addition, some studies utilized very simplified models, which were intuitively modeled

* Associate Professor, Department of Intelligent Machinery and Systems
** Professor, Department of Intelligent Machinery and Systems

as several degrees of freedom systems[8),9)]. However, it is difficult for any methods to estimate the errors between the reduced model and the real structure. In the case of modal reduction, a pretreatment to compute the characteristic modes took considerable computational costs. Thus, computational algorithm with high speed is desirable in order to realize a dynamic response analysis of a large scale structure without a reduction in the degree of freedom.

The Transfer Matrix Method (hereafter: TMM)[10)] is one of the applicable methods. But the TMM is only available to such a structure as illustrated in **Fig. 1(a)**, in which the structure starts with one end and terminates with another end. In addition, the TMM has some disadvantages in treatment of rigid supports and a computation of high frequency range. A deterioration of computational accuracy happens in such cases. In the worst case, the numerical computation diverges.

Sueoka (one of the authors) et al. presented an alternate method, the Transfer Influence Coefficient Method (hereafter: TICM)[11),12)]. The TICM has an advantage in computational accuracy and speed. A remarkable feature of the TICM is its controllability on various boundary conditions only by means of an adjustment of spring constants. No numerical instability happens even if the spring constants become very large, and computational accuracy can be maintained. Such a treatment is inapplicable to the TMM. This advantage of the TICM is also retained in a computation of high frequency range. Furthermore, the TICM has a high computational speed since the dimensions of matrices and vectors used in the algorithm are smaller than the ones of the TMM. The TICM is defeating the disadvantages of the TMM and is applicable to free vibration, forced vibration, transient response, and nonlinear response. However, the treatable structure of the TICM was the same as the TMM. The TICM was not capable of a frame structure schematically illustrated in **Fig. 1(b)**. The structure includes branches and links to form some closed loops, which are essentially involved in truss and rahmen structures. The original TICM was not able to treat the branch and link so that truss and rahmen structures were not treatable.

In this paper, a new algorithm of the TICM to treat a frame structure with closed loops is presented. New concepts to treat the branch and link are innovated in the algorithm and make the TICM applicable to a structure which involves closed loops in itself. The new algorithm still retains the advantages of the original TICM. A pin joint, which is usually modeled as a joint of truss structure, is easily realized only by an adjustment of a spring constant. Such a treatment is not suitable for conventional methods. In addition, computational costs, i.e., storage and time, are reduced by the new algorithm of the TICM, compared with a conventional routine. It contributes greatly to a practical use. The advantages of the TICM are demonstrated through some numerical computations.

Although the algorithm in this study is restricted within an in-plane free vibration of

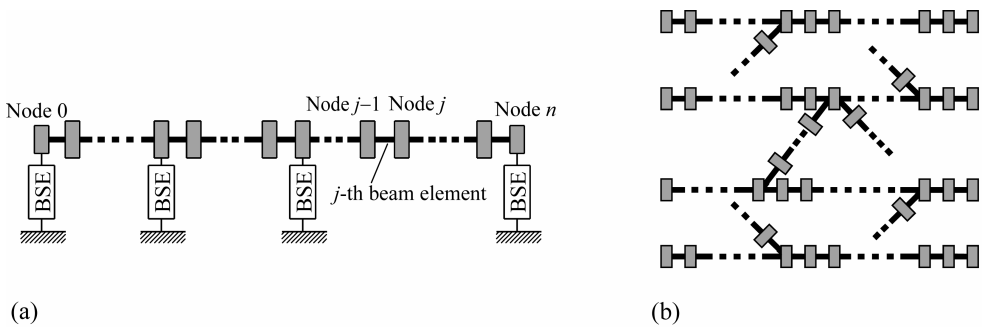

Fig. 1 Schematic diagram of an analytical model. (a) Typical model of the TMM and original TICM and (b) in-plane frame structure with branches and connections.

two-dimensional frame structure in order to simplify the description, the algorithm can be easily extended to three-dimensional structures. Forced vibration, transient response and nonlinear response are also treatable.

2. The Original Algorithm of the Transfer Influence Coefficient Method

The algorithm of the original TICM on the free vibration analysis is briefly mentioned in this section because it is a fundamental part of the new algorithm. A beam structure with no branches and links illustrated in **Fig. 1(a)** is a typical model for the original TICM. A lumped mass system is employed as an analytical model in this paper, but distributed mass modeling is also available. The model is formed by a connection of massless beams and rigid bodies in series. Each rigid body is called "Node" and the left- and the right-hand ends of the system are defined as node 0 and node n, respectively. The beam element between the nodes j and j-1 is called the j-th beam element. Some rigid bodies are supported by base support elements (BSE). The variables with head symbols and subscripts have the following principles.

(1) Variables with subscript j represent the physical quantities related to node j or j-th beam element.

(2) Variables with head symbol " ^ " represent the physical quantities related to a base support element.

(3) Variables with and without head symbol " – " represent the physical quantities on the left- and the right-hand sides of node, respectively.

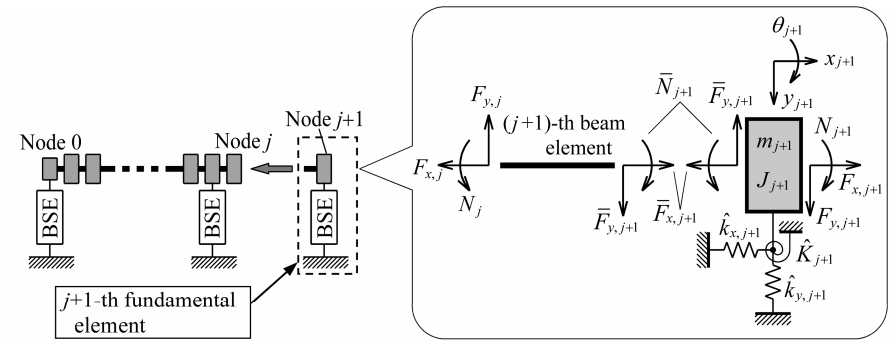

Fig. 2 Schematic diagram of analytical model. (a) Connection of a fundamental element and (b) definition of the positive direction of the state variables.

A connection of (j+1)-th fundamental element to the right-hand side of the node j is shown in **Fig. 2(a)**. The (j+1)-th fundamental element consists of the (j+1)-th beam element, a rigid body and a base support element. This is the concept of the original TICM. Details of the (j+1)-th fundamental element and definition of the positive direction of the state variables are indicated in **Fig. 2(b)**. The system is assumed to be oscillating at an angular frequency ω, and x_{j+1}, y_{j+1} and θ_{j+1} are the amplitudes of axial, lateral displacements and rotation. $F_{x,j+1}$, $F_{y,j+1}$ and N_{j+1} are the amplitudes of axial force, lateral force and bending moment. The relationship of the state variables between both ends of the (j+1)-th beam is represented as:

$$\boldsymbol{d}_{j+1}=(\boldsymbol{L}_{j+1})^{\mathrm{T}}\boldsymbol{d}_j+\boldsymbol{F}_{j+1}\bar{\boldsymbol{f}}_{j+1},\quad \boldsymbol{f}_j=\boldsymbol{L}_{j+1}\bar{\boldsymbol{f}}_{j+1} \tag{1}$$

where right-hand superscript " T " denotes transpose and

$$\boldsymbol{d}_{j+1}=\{x_{j+1}, y_{j+1}, \theta_{j+1}\}^{\mathrm{T}}, \quad \boldsymbol{f}_j=\{F_{x,j}, F_{y,j}, N_j\}^{\mathrm{T}}, \quad \overline{\boldsymbol{f}}_{j+1}=\{\overline{F}_{x,j+1}, \overline{F}_{y,j+1}, \overline{N}_j\}^{\mathrm{T}}$$

$$\boldsymbol{L}_{j+1}=\begin{bmatrix} 1 & 0 & 0 \\ 0 & 1 & 0 \\ 0 & l & 1 \end{bmatrix}_{j+1}, \quad \boldsymbol{F}_{j+1}=\begin{bmatrix} \alpha_x & 0 & 0 \\ 0 & \alpha_y & \gamma \\ 0 & \gamma & \beta \end{bmatrix}_{j+1}, \quad (\alpha_x, \alpha_y, \beta, \gamma)_{j+1}=\left(\frac{l}{EA}, \frac{l^3}{3EI}, \frac{l}{EI}, \frac{l^2}{2EI}\right)_{j+1}$$

l_{j+1}, $(EA)_{j+1}$ and $(EI)_{j+1}$ are length, tensile rigidity and flexural rigidity of (j+1)-th beam. The equation of motion of (j+1)-th rigid body is represented as:

$$\overline{\boldsymbol{f}}_{j+1}+\boldsymbol{P}_{j+1}\boldsymbol{d}_{j+1}=\boldsymbol{f}_{j+1} \tag{2}$$

where

$$\boldsymbol{P}_{j+1}=\hat{\boldsymbol{K}}_{j+1}-\omega^2\boldsymbol{M}_{j+1}, \quad \boldsymbol{M}_{j+1}=\mathrm{diag}(m, m, J)_{j+1}, \quad \hat{\boldsymbol{K}}_{j+1}=\mathrm{diag}(\hat{k}_x, \hat{k}_y, \hat{K})_{j+1}$$

m_{j+1} and J_{j+1} are a mass and a moment of inertia of the (j+1)-th rigid body (node). $\hat{k}_{x,j+1}$, $\hat{k}_{y,j+1}$ are linear spring constants of the x- and y-directions, respectively, and $\hat{K}_{j+1}$ is a rotational spring constant.

In the formulation of the TICM, a relationship between the displacement vector and the force vector at node j is defined as:

$$\boldsymbol{d}_j=\overline{\boldsymbol{T}}_j\overline{\boldsymbol{f}}_j \tag{3a}$$

$$\boldsymbol{d}_j=\boldsymbol{T}_j\boldsymbol{f}_j \tag{3b}$$

where $\overline{\boldsymbol{T}}_j$ and $\boldsymbol{T}_j$ are the dynamic influence coefficient matrices of the left- and the right-hand sides of node j, respectively. These matrices are usually symmetrical. In the algorithm of the TICM, the matrices $\overline{\boldsymbol{T}}_j$ and $\boldsymbol{T}_j$ are successively computed from node 0 to node n.

Substituting Eq. (3b) into Eq. (1) and comparing with Eq. (3a) with subscript j+1, we obtain

$$\overline{\boldsymbol{T}}_{j+1}=(\boldsymbol{L}_{j+1})^{\mathrm{T}}\boldsymbol{T}_j\boldsymbol{L}_{j+1}+\boldsymbol{F}_{j+1} \tag{4}$$

Eliminating $\overline{\boldsymbol{f}}_{j+1}$ from Eq. (2) by utilizing Eq. (3a) with subscript j+1 and comparing with Eq. (3b) with subscript j+1, we obtain

$$(\boldsymbol{I}_3+\overline{\boldsymbol{T}}_{j+1}\boldsymbol{P}_{j+1})\boldsymbol{T}_{j+1}=\overline{\boldsymbol{T}}_{j+1} \tag{5}$$

where $\boldsymbol{I}_3$ is a 3×3 identity matrix. The matrices $\overline{\boldsymbol{T}}_{j+1}$ and $\boldsymbol{T}_{j+1}$ are obtained from $\boldsymbol{T}_j$ through Eqs. (4) and (5) in turn. Furthermore, successive operations of Eqs. (4) and (5) yield $\overline{\boldsymbol{T}}_{j+1}, \boldsymbol{T}_{j+1}, \ldots, \overline{\boldsymbol{T}}_n, \boldsymbol{T}_n$ recursively. The formulations (4) and (5) are called the "field transmission rule" and the "point transmission rule", respectively. The initial dynamic influence coefficient matrix $\boldsymbol{T}_0$ at node 0 is needed first for the successive operations. This matrix is derived from the equilibrium of forces at node 0 as:

$$\boldsymbol{P}_0\boldsymbol{d}_0=\boldsymbol{f}_0 \quad \Rightarrow \quad \boldsymbol{d}_0=\boldsymbol{T}_0\boldsymbol{f}_0, \quad \boldsymbol{P}_0\boldsymbol{T}_0=\boldsymbol{I}_3 \tag{6}$$

Consequently, the dynamic influence coefficient matrices are computed in turn from node 0 to node n by Eq. (6) and recursive operations of Eqs. (4) and (5).

After the computation of $\boldsymbol{T}_j$ ($j=0\rightarrow n$), substituting Eq. (3a) into Eq. (2) with subscript n, we obtain the relationship of the force vectors at node n.

$$(\boldsymbol{I}_3+\boldsymbol{P}_n\overline{\boldsymbol{T}}_n)\overline{\boldsymbol{f}}_n=\boldsymbol{f}_n \tag{7}$$

Since the right-hand side of node n is always free, the force vector at the right-hand side of node n is zero: $\boldsymbol{f}_n=\boldsymbol{0}$. Conversely, the left-hand side of node n is not free, that is $\overline{\boldsymbol{f}}_n\neq\boldsymbol{0}$. Thus, the frequency equation is given by

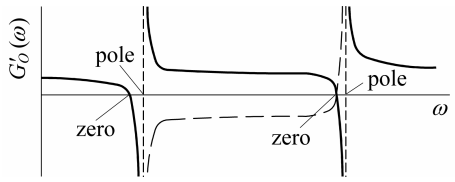

Fig. 3 Asymmetric poles and zeros of $G'_O(\omega)$.

$$G'_O(\omega) \equiv \det(\boldsymbol{I}_3 + \boldsymbol{P}_n \overline{\boldsymbol{T}}_n) = 0 \tag{8a}$$

An angular frequency ω that satisfies Eq. (8a) is a natural angular frequency. The frequency equation (8a) is classified as a determinant method. The bisection method is usually employed to solve the determinant method. However, the frequency equation $G'_O(\omega)$ has asymmetric poles as shown in **Fig. 3** (solid line), which are regarded as pseud-solutions of $G'_O(\omega) = 0$ in a simple application of the bisection method. In our previous study[12], it was confirmed that the asymmetric poles are generated at $\det(\boldsymbol{I}_3 + \overline{\boldsymbol{T}}_j \boldsymbol{P}_j) = 0$ ($j = 1, \ldots, n$) and $\det \boldsymbol{P}_0 = 0$. In other words, the asymmetric poles are generated in the cases that the simultaneous equations of the point transmission rule [Eq. (5)] and the computation of $\boldsymbol{T}_0$ [Eq. (6)] become singular. Hence, the asymmetric poles are transformed into symmetric poles by means of inversion of plus and minus of $G'_O(\omega)$ at the points of $\det(\boldsymbol{I}_3 + \overline{\boldsymbol{T}}_j \boldsymbol{P}_j) = 0$ and $\det \boldsymbol{P}_0 = 0$ as illustrated by broken line in **Fig. 3**. The modified frequency equation is given as follows.

$$G_O(\omega) \equiv \det \boldsymbol{P}_0 \prod_{j=1}^{n} \det(\boldsymbol{I}_3 + \overline{\boldsymbol{T}}_j \boldsymbol{P}_j) = 0 \tag{8b}$$

where the symmetry of the matrix $\overline{\boldsymbol{T}}_n$ and $\boldsymbol{P}_n$ are utilized. The computation of $\det(\boldsymbol{I}_3 + \overline{\boldsymbol{T}}_j \boldsymbol{P}_j) = 0$ and $\det \boldsymbol{P}_0 = 0$ are accompanied with the Eqs. (5) and (6), so that no computational costs increase. Only the zeros of $G_O(\omega)$ are obtained by a simple application of the bisection method to Eq. (8b).

Once a natural angular frequency is obtained from Eq. (8b), the force vector $\overline{\boldsymbol{f}}_n$ is determined by Eq. (7) with one fixed element (usually 1) since $\boldsymbol{f}_n = \boldsymbol{0}$. The displacement vector at node n is given by $\boldsymbol{d}_n = \overline{\boldsymbol{T}}_n \overline{\boldsymbol{f}}_n$. The rest of the displacement vectors are recursively obtained from node $n-1$ to node 0 by applying the following equations, which are derived from Eqs. (1), (2) and (3b).

$$\boldsymbol{f}_{j-1} = \boldsymbol{L}_j \overline{\boldsymbol{f}}_j, \quad \boldsymbol{d}_{j-1} = \boldsymbol{T}_{j-1} \boldsymbol{f}_{j-1}, \quad \overline{\boldsymbol{f}}_{j-1} = \boldsymbol{f}_{j-1} - \boldsymbol{P}_{j-1} \boldsymbol{d}_{j-1} \quad (j = n \to 1) \tag{9}$$

Finally, all the displacement vectors $\boldsymbol{d}_j$ $(j = n \to 0)$ correspond to a characteristic mode.

The algorithm of the TICM is available if the spring constants $\hat{k}_{x,j}$, $\hat{k}_{y,j}$ or $\hat{K}_j$ become very large because the TICM treats the physical quantities as influence coefficients (inverse of rigidity). The TICM is also available if the spring constants are equal to zero. Apparently Eqs. (4) and (5) are available in such a case, and Eq. (6) is also available because an inertial term $-\omega^2 \boldsymbol{M}_0$ always exists in $\boldsymbol{P}_0$. The TICM is numerically powerful in any situation and keeps high computational accuracy. This character comes to the advantage of the TICM that various boundary conditions are realized only by an adjustment of spring constants.

3. New Algorithm of the Transfer Influence Coefficient Method

A large scale frame structure such as a long span bridge consists of several main systems, and subsystems which link the main systems to each other. An example is diagrammatically illustrated in **Fig. 4**. It represents a general in-plane frame structure which includes branches and links to form closed loops. A lumped mass system is also applied to model the system, and the number of the

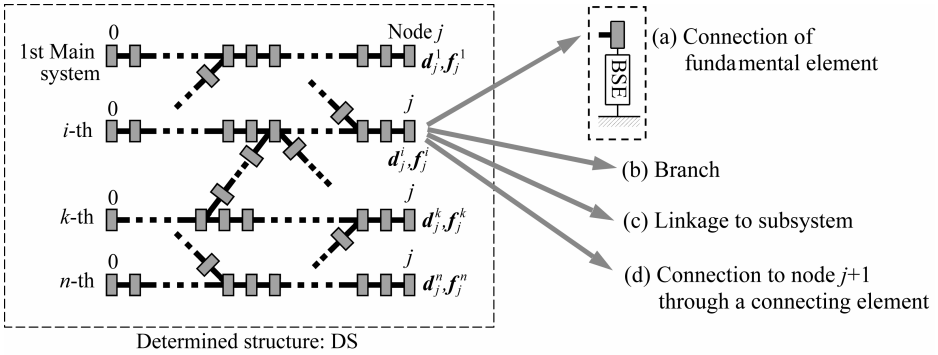

Fig. 4 Concept of the newly presented TICM.

main system is assumed to be n. A subsystem branches from a certain point of the main system and links to the other main system. Although a case that a subsystem branches further into two or more system is available, the algorithm in this paper is formulated on the assumption that only a main system branches. The system is partly supported by a base support element, which is not depicted in **Fig. 4**.

In the new algorithm, a dynamic influence coefficient matrix is defined as well as the original algorithm. The computation of the dynamic influence coefficient matrix also begins at the left-hand side of the system, and proceeds to the right-hand side of the system as a whole. The rigid bodies are also defined as node 0, 1, ⋯ , in turn from the left-hand side of a main system. As for a subsystem, node 0 corresponds to a branch point from a main system. Variables with head symbols and subscripts in this section are common to Section 2, but variables with superscript "i" represents the physical quantities related to the i-th main system, and superscript "sub" represents the ones related to subsystems.

The structure enclosed with a broken line in **Fig. 4** is defined as a determined structure (hereafter: DS). In the DS, only the node j of each main system is allowed to connect with a fundamental element, branch, link to a subsystem, etc., as listed in **Figs. 4 (a)–(d)**. The repetition of the process leads to the completion of the whole structure. This is a concept of the new algorithm of the TICM. In the new algorithm, a relationship between a displacement vector and a force vector of the DS is defined as:

$$\boldsymbol{d} = \boldsymbol{T}\boldsymbol{f} \tag{10}$$

where

$$\begin{aligned} &\boldsymbol{d} = \{(\boldsymbol{d}_j^1)^{\mathrm{T}}, \cdots, (\boldsymbol{d}_j^i)^{\mathrm{T}}, \cdots, (\boldsymbol{d}_j^n)^{\mathrm{T}}\}^{\mathrm{T}}, \quad \boldsymbol{f} = \{(\boldsymbol{f}_j^1)^{\mathrm{T}}, \cdots, (\boldsymbol{f}_j^i)^{\mathrm{T}}, \cdots, (\boldsymbol{f}_j^n)^{\mathrm{T}}\}^{\mathrm{T}} \\ &\boldsymbol{d}_j^i = \{x_j^i, y_j^i, \theta_j^i\}^{\mathrm{T}}, \quad \boldsymbol{f}_j^i = \{F_{x,j}^i, F_{y,j}^i, N_j^i\}^{\mathrm{T}} \end{aligned} \tag{11}$$

The degree of freedom of $\boldsymbol{d}$ and $\boldsymbol{f}$ is $3n$, while $\boldsymbol{T}$ is a $3n \times 3n$ square matrix.

3.1 Field and point transmission rules

Supposing that node j of the i-th main system connects with a fundamental element as shown in **Fig. 4(a)**, the field and point transmission rule of Eqs. (4) and (5) are easily extended to this case.

$$\overline{\boldsymbol{T}} = (\boldsymbol{L})^{\mathrm{T}}\boldsymbol{T}\boldsymbol{L} + \boldsymbol{F} \tag{12}$$

$$(\boldsymbol{I}_{3n} + \overline{\boldsymbol{T}}\boldsymbol{P})\boldsymbol{T}' = \overline{\boldsymbol{T}} \tag{13}$$

where

$$\begin{aligned}&\boldsymbol{L}=\mathrm{Diag}[\boldsymbol{I}_3,\cdots,\boldsymbol{I}_3,\boldsymbol{L}^i_{j+1},\boldsymbol{I}_3,\cdots,\boldsymbol{I}_3],\quad \boldsymbol{F}=\mathrm{Diag}[\boldsymbol{0}_3,\cdots,\boldsymbol{0}_3,\boldsymbol{F}^i_{j+1},\boldsymbol{0}_3,\cdots,\boldsymbol{0}_3]\\&\boldsymbol{P}=\mathrm{Diag}[\boldsymbol{0}_3,\cdots,\boldsymbol{0}_3,\boldsymbol{P}^i_{j+1},\boldsymbol{0}_3,\cdots,\boldsymbol{0}_3]\end{aligned}\tag{14}$$

$\boldsymbol{I}_{3n}$ is a $3n\times3n$ identity matrix and $\boldsymbol{0}_3$ is a 3×3 zero matrix. All the diagonal blocks of $\boldsymbol{L}$ are 3×3 identity matrices but the i-th block is $\boldsymbol{L}^i_{j+1}$. All the diagonal blocks of $\boldsymbol{F}$ and $\boldsymbol{P}$ are 3×3 zero matrices but the i-th block is $\boldsymbol{F}^i_{j+1}$ and $\boldsymbol{P}^i_{j+1}$, respectively. Each of $\boldsymbol{L}$, $\boldsymbol{F}$ and $\boldsymbol{P}$ is a $3n\times3n$ square matrix. The block elements $\boldsymbol{L}^i_{j+1}$, $\boldsymbol{F}^i_{j+1}$ and $\boldsymbol{P}^i_{j+1}$ are represented as a same formula as $\boldsymbol{L}_{j+1}$, $\boldsymbol{F}_{j+1}$ and $\boldsymbol{P}_{j+1}$ of Eqs. (1) and (2), respectively. These matrices satisfy the following formula, similar to Eqs. (1) and (2).

$$\boldsymbol{d}_{j+1}=(\boldsymbol{L}^i_{j+1})^{\mathrm{T}}\boldsymbol{d}_j+\boldsymbol{F}^i_{j+1}\overline{\boldsymbol{f}}_{j+1},\quad \boldsymbol{f}_j=\boldsymbol{L}^i_{j+1}\overline{\boldsymbol{f}}_{j+1}\tag{15a}$$

$$\begin{aligned}&\overline{\boldsymbol{f}}^i_{j+1}+\boldsymbol{P}^i_{j+1}\boldsymbol{d}^i_{j+1}=\boldsymbol{f}^i_{j+1}\\&\boldsymbol{P}^i_{j+1}=\hat{\boldsymbol{K}}^i_{j+1}-\omega^2\boldsymbol{M}^i_{j+1},\quad \boldsymbol{M}^i_{j+1}=\mathrm{diag}(m,m,J)^i_{j+1},\quad \hat{\boldsymbol{K}}^i_{j+1}=\mathrm{diag}(\hat{k}_x,\hat{k}_y,\hat{K})^i_{j+1}\end{aligned}\tag{15b}$$

The dynamic influence coefficient matrices $\overline{\boldsymbol{T}}$ and $\boldsymbol{T}'$ satisfy the following relationships:

$$\boldsymbol{d}'=\overline{\boldsymbol{T}}\overline{\boldsymbol{f}},\qquad \boldsymbol{d}'=\{(\boldsymbol{d}^1_j)^{\mathrm{T}},\cdots,(\boldsymbol{d}^i_{j+1})^{\mathrm{T}},\cdots,(\boldsymbol{d}^n_j)^{\mathrm{T}}\}^{\mathrm{T}},\quad \overline{\boldsymbol{f}}=\{(\boldsymbol{f}^1_j)^{\mathrm{T}},\cdots,(\overline{\boldsymbol{f}}^i_{j+1})^{\mathrm{T}},\cdots,(\boldsymbol{f}^n_j)^{\mathrm{T}}\}^{\mathrm{T}}\tag{16a}$$

$$\boldsymbol{d}'=\boldsymbol{T}'\boldsymbol{f}',\qquad \boldsymbol{f}'=\{(\boldsymbol{f}^1_j)^{\mathrm{T}},\cdots,(\boldsymbol{f}^i_{j+1})^{\mathrm{T}},\cdots,(\boldsymbol{f}^n_j)^{\mathrm{T}}\}^{\mathrm{T}}\tag{16b}$$

The elements of $\boldsymbol{L}$, $\boldsymbol{F}$ and $\boldsymbol{P}$ are properly substituted if a fundamental element connects to the other main system.

3.2 Transformation of coordinates

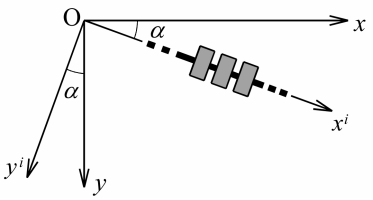

Fig. 5 Transformation of coordinate.

The new algorithm of the TICM is formulated on the assumption that the axial direction of the beam element coincides with the x-axis. However, all the axial directions of beam elements are not the same. Thus, physical quantities have to be treated in a common coordinate. Supposing that the coordinate of the i-th main system O-x^iy^i inclines against a common coordinate O-xy at an angle of α as shown in **Fig. 5**, the physical quantities indicated in O-x^iy^i are transformed into the ones in O-xy. The matrices $\boldsymbol{L}^i_{j+1}$, $\boldsymbol{F}^i_{j+1}$ and $\boldsymbol{P}^i_{j+1}$ indicated in O-x^iy^i are transformed as follows:

$$\begin{aligned}&\boldsymbol{R}\boldsymbol{L}^i_{j+1}\boldsymbol{R}^{\mathrm{T}}\Rightarrow\boldsymbol{L}^i_{j+1}\\&\boldsymbol{R}\boldsymbol{F}^i_{j+1}\boldsymbol{R}^{\mathrm{T}}\Rightarrow\boldsymbol{F}^i_{j+1}\\&\boldsymbol{R}\boldsymbol{P}^i_{j+1}\boldsymbol{R}^{\mathrm{T}}\Rightarrow\boldsymbol{P}^i_{j+1}\end{aligned}\qquad \boldsymbol{R}=\begin{bmatrix}\cos\alpha & -\sin\alpha & 0\\ \sin\alpha & \cos\alpha & 0\\ 0 & 0 & 1\end{bmatrix}\tag{17}$$

The discussion in this paper is supposed to be done under the condition that all the matrices $\boldsymbol{L}^i_{j+1}$, $\boldsymbol{F}^i_{j+1}$ and $\boldsymbol{P}^i_{j+1}$ are transformed by Eq. (17). The displacement vectors, force vectors and dynamic influence coefficient matrices are automatically indicated in the common coordinate under the transformation.

3.3 Branch transmission rule

If the DS in **Fig. 4** is fixed, the dynamic influence coefficient matrix $\boldsymbol{T}$ of Eq. (10) is determined. A case that a subsystem branches from node j of the i-th main system as shown in **Fig. 4(b)** is

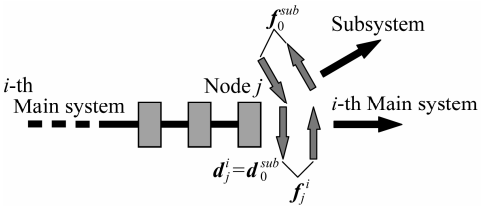

Fig. 6 Diagram of branch.

considered in this section. A schematic diagram of the branch is illustrated in **Fig. 6**. Although the directions of $\boldsymbol{f}_j^i$ and $\boldsymbol{f}_0^{sub}$ seem to be different from each other, the force vectors are actually represented in the common coordinate discussed in Section 3.2. The force vectors in **Figs. 7**, **9** and **10** are similarly represented. The subscript "0" of $\boldsymbol{f}_0^{sub}$ denotes physical quantities of the left-hand side of the subsystem. Since the branch generates a new force vector $\boldsymbol{f}_0^{sub}$, which acts on node j of the i-th main system from the subsystem, a new force vector after the branch is defined as follows:

$$\boldsymbol{f}^{sub} = \{(\boldsymbol{f}_j^1)^{\mathrm{T}}, \cdots, (\boldsymbol{f}_j^i)^{\mathrm{T}}, \cdots, (\boldsymbol{f}_j^n)^{\mathrm{T}}, (\boldsymbol{f}_0^{sub})^{\mathrm{T}}\}^{\mathrm{T}}$$

An extra block for the subsystem $(\boldsymbol{f}_0^{sub})^{\mathrm{T}}$ is added to $\boldsymbol{f}^{sub}$. Since node j of the i-th main system is subjected to both force vectors $\boldsymbol{f}_j^i$ and $\boldsymbol{f}_0^{sub}$, the following formula substitutes for Eq. (10) after the branch.

$$\boldsymbol{d} = \boldsymbol{T}\boldsymbol{B}^{\mathrm{T}} \boldsymbol{f}^{sub}, \qquad \boldsymbol{B} = \begin{bmatrix} \boldsymbol{I}_3 & \ddots & & \boldsymbol{0} \\ & & \boldsymbol{I}_3 & \\ \boldsymbol{0} & & & \ddots \\ & & & \boldsymbol{I}_3 \\ \cdots\ \boldsymbol{0}_3 & & \boldsymbol{I}_3 & \boldsymbol{0}_3\ \cdots \end{bmatrix} \quad (18)$$

(i-th block of column)

where the matrix $\boldsymbol{B}$ is a $3(n+1)\times 3n$ matrix.

A new displacement vector after the branch is defined according to the definition of $\boldsymbol{f}^{sub}$ as follows:

$$\boldsymbol{d}^{sub} = \{(\boldsymbol{d}_j^1)^{\mathrm{T}}, \cdots, (\boldsymbol{d}_j^i)^{\mathrm{T}}, \cdots, (\boldsymbol{d}_j^n)^{\mathrm{T}}, (\boldsymbol{d}_0^{sub})^{\mathrm{T}}\}^{\mathrm{T}}$$

where $\boldsymbol{d}_0^{sub}$ is a displacement vector of the left-hand side of the subsystem. Apparently $\boldsymbol{d}_j^i = \boldsymbol{d}_0^{sub}$ since node j of the i-th main system is identical to the left-hand side of the subsystem. Thus, $\boldsymbol{d}^{sub}$ is represented as: $\boldsymbol{d}^{sub} = \boldsymbol{B}\boldsymbol{d}$. Substituting Eq. (18) into the relation $\boldsymbol{d}^{sub} = \boldsymbol{B}\boldsymbol{d}$ yields

$$\boldsymbol{d}^{sub} = \boldsymbol{T}^{sub} \boldsymbol{f}^{sub}, \qquad \boldsymbol{T}^{sub} = \boldsymbol{B}\boldsymbol{T}\boldsymbol{B}^{\mathrm{T}} \quad (19)$$

The $3(n+1)\times 3(n+1)$ square matrix $\boldsymbol{T}^{sub}$ associates the displacement vector $\boldsymbol{d}^{sub}$ with the force vector $\boldsymbol{f}^{sub}$, so that the matrix $\boldsymbol{T}^{sub}$ corresponds to a dynamic influence coefficient matrix after the branch. We call Eq. (19) the "branch transmission rule".

After the branch, the subsystem extends to node 1, 2, ···, and the field and point transmission rules in Section 3.1 are available to the extension. The elements of $\boldsymbol{B}$ are properly substituted if a subsystem branches from the other main system.

3.4 Mutual joint transmission rule

Supposing that a subsystem branches from a main system (except the i-th main system) and reaches node q, the displacement vector of $\boldsymbol{d}^{sub}$ is newly represented as:

$$\boldsymbol{d}^{sub} \Leftarrow \{(\boldsymbol{d}_j^1)^{\mathrm{T}}, \cdots, (\boldsymbol{d}_j^i)^{\mathrm{T}}, \cdots, (\boldsymbol{d}_j^n)^{\mathrm{T}}, (\boldsymbol{d}_q^{sub})^{\mathrm{T}}\}^{\mathrm{T}}$$

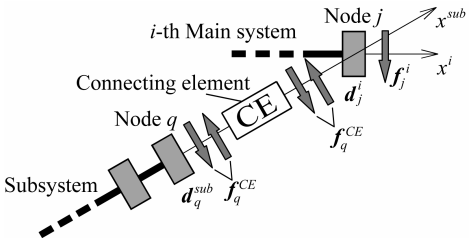

Fig. 7 Diagram of mutual joint.

Note that $\boldsymbol{d}_0^{sub}$ in $\boldsymbol{d}^{sub}$ just after the branch discussed in Section 3.3 transfers into $\boldsymbol{d}_q^{sub}$. The dynamic influence coefficient matrix on this condition, which is denoted $\boldsymbol{T}^{sub}$, is obtained through the brunch, field and point transmission rules. Then, the node q of the subsystem connects with node j of the i-th main system through a connecting element (CE). A schematic diagram of the connection is illustrated in **Fig. 7**. The subsystem links to the i-th main system by the connection, which corresponds to a description of **Fig. 4(c)**. We call it a "Mutual joint" in this paper. The i-th main system still extends toward the right-hand side of the system after the connection, while the subsystem is terminated with the connection. Hence, the node q of the subsystem is only subjected to the inner force vector $\boldsymbol{f}_q^{CE}$, while node j of the i-th main system is subjected to $\boldsymbol{f}_q^{CE}$ and $\boldsymbol{f}_j^i$. The relationship between the displacement and force vector is represented as follows:

$$\begin{aligned}
&\boldsymbol{d}^{sub} = \boldsymbol{T}^{sub}(\boldsymbol{f}^{sub} + \boldsymbol{f}^{CE}) \\
&\boldsymbol{f}^{sub} = \{(\boldsymbol{f}_j^1)^{\mathrm{T}}, \cdots, (\boldsymbol{f}_j^i)^{\mathrm{T}}, \cdots \cdots, (\boldsymbol{f}_j^n)^{\mathrm{T}}, \{0_3\}\}^{\mathrm{T}} \\
&\boldsymbol{f}^{CE} = \{\cdots, \{0_3\}, -(\boldsymbol{f}_q^{CE})^{\mathrm{T}}, \{0_3\}, \cdots, \{0_3\}, (\boldsymbol{f}_q^{CE})^{\mathrm{T}}\}^{\mathrm{T}} \\
&\qquad\qquad i\text{-th block}
\end{aligned} \tag{20}$$

where $\{0_3\}=(0,0,0)$. The $3(n+1)$ force vector $\boldsymbol{f}^{CE}$ represents the inner force from the CE ,while $\boldsymbol{f}^{sub}$ represents the force vectors which act on the node j of all the main systems. All the blocks of $\boldsymbol{f}^{CE}$ are zero but the i-th and the $(n+1)$-th blocks are $-(\boldsymbol{f}_q^{CE})^{\mathrm{T}}$ and $(\boldsymbol{f}_q^{CE})^{\mathrm{T}}$, respectively. The minus sign of $-(\boldsymbol{f}_q^{CE})^{\mathrm{T}}$ is due to an opposite definition of the positive direction of $\boldsymbol{f}_q^{CE}$ to the direction of $\boldsymbol{f}_j^i$ in a common coordinate. The $(n+1)$-th block of $\boldsymbol{f}^{sub}$, which is prepared for the subsystem, is zero since the inner force vector $\boldsymbol{f}_q^{CE}$ is included in $\boldsymbol{f}^{CE}$.

The inner force vector $\boldsymbol{f}_q^{CE}$ is associated with the displacement vectors $\boldsymbol{d}_j^i$ and $\boldsymbol{d}_q^{sub}$ as:

$$\boldsymbol{f}_q^{CE} = \boldsymbol{K}^{CE}(\boldsymbol{d}_j^i - \boldsymbol{d}_q^{sub}) \tag{21}$$

where $\boldsymbol{K}^{CE}$ represents a stiffness matrix of the CE. Eliminating the inner force vector $\boldsymbol{f}^{CE}$ from Eq. (20) by substituting Eq. (21) yields

$$\boldsymbol{d}^{sub} = \boldsymbol{T}^{sub\text{-}i}\boldsymbol{f}, \qquad (\boldsymbol{U}^{-1} + \boldsymbol{T}^{sub}\boldsymbol{K}^{mu})\boldsymbol{U}\boldsymbol{T}^{sub\text{-}i} = \boldsymbol{T}^{sub} \tag{22}$$

$$\boldsymbol{U} = \left[\begin{array}{ccc:c:c} \boldsymbol{I}_3 & & & \cdots & \boldsymbol{0} \\ & \ddots & & & \vdots \\ & & \boldsymbol{I}_3 & & \\ \vdots & & & \ddots & \\ \boldsymbol{0} & \cdots & -\boldsymbol{I}_3 & \boldsymbol{0} & \boldsymbol{I}_3 \end{array}\right], \quad \boldsymbol{K}^{mu} = \left[\begin{array}{ccc:c} & & & \vdots \\ & & & \boldsymbol{0}_3 \\ \hdashline & \boldsymbol{0} & & -\boldsymbol{K}^{CE} \\ \hdashline & & \ddots & \boldsymbol{0}_3 \\ & & & \vdots \\ \hdashline \boldsymbol{0}_3 & \cdots & \boldsymbol{0}_3 & \boldsymbol{K}^{CE} \end{array}\right] \leftarrow i\text{-th block of row}$$

i-th block of column

All the elements of $\boldsymbol{U}$ are zero but the diagonal blocks are $\boldsymbol{I}_3$ besides $(n+1)$-i block is $-\boldsymbol{I}_3$. Replacing $-\boldsymbol{I}_3$ of $\boldsymbol{U}$ by $\boldsymbol{I}_3$ represents $\boldsymbol{U}^{-1}$. All the elements of $\boldsymbol{K}^{mu}$ are zero but the i-$(n+1)$ block and the $(n+1)$-$(n+1)$ blocks are $-\boldsymbol{K}^{CE}$ and $\boldsymbol{K}^{CE}$, respectively. The matrix $\boldsymbol{T}^{sub\text{-}i}$, which is derived from Eq. (22), is a dynamic influence coefficient matrix after the mutual joint, and we call Eq. (22)

the "mutual joint transmission rule". The elements of $\boldsymbol{U}$ and $\boldsymbol{K}^{mu}$ are properly substituted if the subsystem links to the other main system.

A formula $(\boldsymbol{I}_{3(n+1)}+\boldsymbol{T}^{sub}\boldsymbol{K}^{mu}\boldsymbol{U})\boldsymbol{T}^{sub\text{-}i}=\boldsymbol{T}^{sub}$, where $\boldsymbol{I}_{3(n+1)}$ is a $3(n+1)$ identity matrix, is possible to substitute for Eq. (22), but the formula (22) is desirable because it is free from a numerical instability even if the elements of $\boldsymbol{K}^{CE}$ take large values. It follows that various connecting elements, for example a pin joint, sliding, etc., are realized only by adjusting the spring constants of $\boldsymbol{K}^{CE}$. Supposing that the stiffness matrix is represented as $\boldsymbol{K}^{CE}=\mathrm{diag}(k_x^{CE},k_y^{CE},K^{CE})$, some examples of connecting elements are given as follows:

· pin joint : $k_x^{CE},k_y^{CE}\to\infty$, $K^{CE}=0$.
· rigid connection : $k_x^{CE},k_y^{CE},K^{CE}\to\infty$.
· sliding (in the *x*-direction): $k_x^{CE}=0$, $k_y^{CE},K^{CE}\to\infty$.
· pin joint with sliding (in the *x*-direction): $k_x^{CE},K^{CE}=0$, $k_y^{CE}\to\infty$.

In the case that the sliding moves in the *y*-direction, k_x^{CE} is alternated with k_y^{CE}. If the direction of k_x^{CE},k_y^{CE} inclines at a angle of α against the common coordinate O-*xy*, the coordinate of $\boldsymbol{K}^{CE}$ is transformed to the common coordinate as $\boldsymbol{R}\boldsymbol{K}^{CE}\boldsymbol{R}^{\mathrm{T}}\Rightarrow\boldsymbol{K}^{CE}$.

After the link of the subsystem to a main system, the system consequently returns to the DS of **Fig. 4** since the subsystem is terminated by the connection. It follows that rearrangements of $\boldsymbol{d}^{sub}$, $\boldsymbol{f}^{sub}$ and $\boldsymbol{T}^{sub\text{-}i}$ to eliminate the degree of freedom associated with the subsystem is necessary. The vectors and matrix $\boldsymbol{d}^{sub}$, $\boldsymbol{f}^{sub}$ and $\boldsymbol{T}^{sub\text{-}i}$ return to $\boldsymbol{d}$, $\boldsymbol{f}$ and $\boldsymbol{T}$ in Eqs. (10) and (11) by following operation:

$$\begin{aligned}&\boldsymbol{C}\boldsymbol{d}^{sub}\Rightarrow\boldsymbol{d}\\&\boldsymbol{C}\boldsymbol{f}^{sub}\Rightarrow\boldsymbol{f}\\&\boldsymbol{C}\boldsymbol{T}^{sub\text{-}i}\boldsymbol{C}^{\mathrm{T}}\Rightarrow\boldsymbol{T},\end{aligned}\qquad \boldsymbol{C}=\begin{bmatrix}\boldsymbol{I}_3 & & \cdots & \boldsymbol{0}\\ & \boldsymbol{I}_3 & & \vdots\\ \vdots & & \ddots & \vdots\\ \boldsymbol{0} & \cdots & \boldsymbol{I}_3 & \boldsymbol{0}\end{bmatrix} \tag{23}$$

where $\boldsymbol{C}$ is a $3n\times3(n+1)$ transform matrix.

3.5 Self joint transmission rule

Connecting elements such as pin and sliding do not exist only in a joint between subsystem and main system, but also other points in a system. A schematic diagram of the connection in a main system or subsystem is illustrated in **Fig. 8(a)**, in which node *j* of the *i*-th main system connects to next node *j*+1 through a CE. We call it a "Self joint" in this paper, and it corresponds to a description of **Fig. 4(d)**. Supposing that the CE consists of a stiffness matrix $\boldsymbol{K}^{CE}$ as same as mutual joint, the transmission rule through the CE is obtained by eliminating $\boldsymbol{d}_j$ from Eq. (10) according to a relationship of $\boldsymbol{f}_j^i=\bar{\boldsymbol{f}}_{j+1}^i=\boldsymbol{K}^{CE}(\boldsymbol{d}_{j+1}^i-\boldsymbol{d}_j^i)$ as:

$$\bar{\boldsymbol{T}}=\boldsymbol{T}+\boldsymbol{G}^{self},\qquad \boldsymbol{G}^{self}=\mathrm{Diag}[\cdots,\underset{i\text{-th block}}{\boldsymbol{0}_3,(\boldsymbol{K}^{CE})^{-1}},\boldsymbol{0}_3,\cdots] \tag{24}$$

The matrix $\boldsymbol{G}^{self}$ is a $3n\times3n$ square matrix. All the diagonal blocks of $\boldsymbol{G}^{self}$ are zero, but the *i*-th

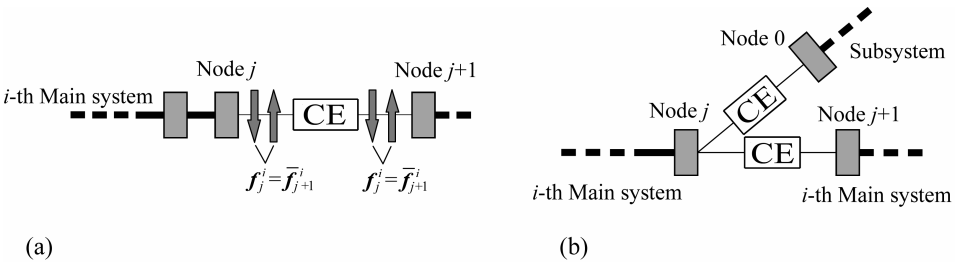

(a) (b)

Fig. 8 Self joint: (a) Diagram and (b) branch point with self joint.

block is $(\boldsymbol{K}^{CE})^{-1}$. A direct use of Eq. (24) is unavailable because there is a possibility that the stiffness matrix $\boldsymbol{K}^{CE}$ becomes singular. An available alternate is a concurrent operation of Eq. (24) with the point transmission rule Eq. (13). Substituting Eq. (24) into Eq. (13) and multiplying the *i*-th block by $\boldsymbol{K}^{CE}$ from the left-hand side yields

$$[\boldsymbol{K}^{self}+(\boldsymbol{K}^{self}\boldsymbol{T}+\boldsymbol{E})\boldsymbol{P}]\,\boldsymbol{T}'=\boldsymbol{K}^{self}\boldsymbol{T}+\boldsymbol{E} \tag{25}$$

$$\boldsymbol{K}^{self}=\mathrm{Diag}[\cdots,\boldsymbol{I}_3,\underset{i\text{-th block}}{\boldsymbol{K}^{CE}},\boldsymbol{I}_3,\cdots],\quad \boldsymbol{E}=\mathrm{Diag}[\cdots,\boldsymbol{0}_3,\underset{i\text{-th block}}{\boldsymbol{I}_3},\boldsymbol{0}_3,\cdots]$$

The matrices $\boldsymbol{K}^{self}$ and $\boldsymbol{E}$ are $3n\times3n$ square matrices. All the diagonal blocks of $\boldsymbol{K}^{self}$ are 3×3 unit matrices, but the *i*-th block is $\boldsymbol{K}^{CE}$. All the diagonal blocks of $\boldsymbol{E}$ are 3×3 zero matrices, but the *i*-th block is $\boldsymbol{I}_3$. Since the matrix $\boldsymbol{T}'$ obtained by Eq. (25) is a dynamic influence coefficient matrix through the self joint, we call Eq. (25) the "self joint transmission rule". If the stiffness matrix $\boldsymbol{K}^{CE}$ is similarly represented as $\boldsymbol{K}^{CE}=\mathrm{diag}(k_x^{CE},k_y^{CE},K^{CE})$, various connecting elements are also realized by adjusting the spring constants as listed in Section 3.4. If necessary, the coordinate of $\boldsymbol{K}^{CE}$ is transformed into the common coordinate.

In a truss structure, branch and linking points are usually modeled as a pin joint. A diagram of the pin joint at a branch is illustrated in **Fig. 8(b)**, where the CE represents a pin joint. The self joint transmission rule is also available in this case, and applied to both the subsystem and the *i*-th main system after the branch. As for a pin joint at a mutual linking, we have already discussed it in Section 3.4.

Consequently, we have obtained a new algorithm of the TICM, i.e., transmission rules on point and field in Section 3.1, a branch in Section 3.3, a mutual joint in Section 3.4, and a self joint in this section. Branches and links to form closed loops are treatable by utilizing the branch and mutual joint transmission rule. In addition, various connecting elements including a pin joint are realized by the mutual and self joint transmission rules with adequately adjusted spring constants. Various support conditions of the base support element such as simply support, rigid support, etc., are also possible. The support conditions are easily realized by adjusting the spring constants of $\hat{\boldsymbol{K}}_{j+1}^{i}$ [Eq. (15b)].

3.6 Treatment of the left-hand side of the system

A successive computation of the dynamic influence coefficient matrix starts from the left-hand side of the whole system. Since the left-hand side of the system consists of the node 0 of each main system as shown in **Fig. 4**, the initial matrix of the dynamic influence coefficient $\boldsymbol{T}_0$ is given in the same manner of the original algorithm [Eq. (6)] as follows:

$$\boldsymbol{P}_0\boldsymbol{T}_0=\boldsymbol{I}_{3n},\qquad \boldsymbol{P}_0=\mathrm{Diag}[\boldsymbol{P}_0^1,\cdots,\boldsymbol{P}_0^i,\cdots,\boldsymbol{P}_0^n] \tag{26}$$

Generally, there are some routes to compute the dynamic influence coefficient matrix toward the right-hand side of the system. In a decision of the route, the most important thing is to keep the dimension of the dynamic influence coefficient matrix as small as possible for saving the computational cost. A practical example to an analytical model is shown in Section 4.

3.7 Frequency equation

Eliminating $\boldsymbol{d}'$ from Eq. (16a) by utilizing Eq.(15b), $\boldsymbol{P}$ of Eq. (14) and $\boldsymbol{f}'$ of Eq. (16b), we obtain

$$(\boldsymbol{I}_{3n}+\boldsymbol{P}\overline{\boldsymbol{T}})\overline{\boldsymbol{f}}=\boldsymbol{f}' \tag{27a}$$

which gives a relationship between the force vectors $\overline{\boldsymbol{f}}$ and $\boldsymbol{f}'$, before and after the point transmission rule. Eliminating $\boldsymbol{d}^{sub}$ from Eq. (20) by utilizing Eq. (21), we have

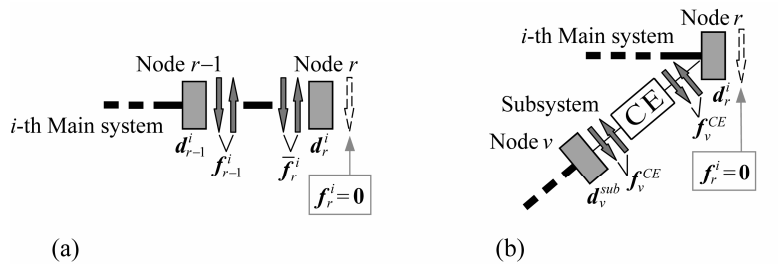

Fig. 9 Termination of the system: (a) Case 1 and (b) case 2.

$$((\boldsymbol{U}^{-1})^{\mathrm{T}}+(\boldsymbol{K}^{mu})^{\mathrm{T}}\boldsymbol{T}^{sub})\boldsymbol{f}^{CE}=-(\boldsymbol{K}^{mu})^{\mathrm{T}}\boldsymbol{T}^{sub}\boldsymbol{f}^{sub} \tag{27b}$$

which gives a relationship between the force vectors $\boldsymbol{f}^{CE}$ and $\boldsymbol{f}^{sub}$ associated with the mutual joint transmission rule. The dynamic influence coefficient matrices are successively computed from the left-hand side to the right-hand side of the system. The final step to complete the computation is classified into following two cases:

(*Case 1*) : a connection of a node as shown in **Fig. 9(a)**, where node *r* of the *i*-th main system is the final node to accomplish the whole system.

(*Case 2*) : a mutual joint of a main system and a subsystem as shown in **Fig. 9(b)**, where a connection of the node *v* of the subsystem with node *r* of the *i*-th main system is a final process to accomplish the whole system.

In case 1, Eq. (27a) is available and $\boldsymbol{f}'=\boldsymbol{0}$ since the right-hand side of the complete system is free. In case 2, Eq. (27b) is available and $\boldsymbol{f}^{sub}=\boldsymbol{0}$ because of the same reason as in case 1. Conversely, $\bar{\boldsymbol{f}}\neq\boldsymbol{0}$ and $\boldsymbol{f}^{CE}\neq\boldsymbol{0}$ in cases 1 and 2, respectively. Thus, a frequency equation is separately given in each case as:

$$Case\,1: G_1(\omega)\equiv\det(\boldsymbol{I}_{3n}+\boldsymbol{P}\bar{\boldsymbol{T}})=0,\quad Case\,2: G_2(\omega)\equiv\det((\boldsymbol{U}^{-1})^{\mathrm{T}}+(\boldsymbol{K}^{mu})^{\mathrm{T}}\boldsymbol{T}^{sub})=0 \tag{28a}$$

The determinant $G_1(\omega)$ and $G_2(\omega)$ also have asymmetric poles as well as $G_O'(\omega)$ [Eq. (8a)] of the original algorithm. It is desirable to eliminate the asymmetric poles in order to exclude pseud-solutions of Eq. (28a). In the newly presented algorithm, the asymmetric poles are also generated in the cases that the simultaneous equations of the transmission rules, i.e., Eqs. (13), (22), (25) and (26) become singular. Consequently, the asymmetric poles are transformed into symmetric poles in the same manner of the original algorithm.

$$\begin{aligned}G(\omega)\equiv\det(\boldsymbol{P}_0)&\prod_{M_1=1}^{N_{point}}\det(\boldsymbol{I}_{3n}+\bar{\boldsymbol{T}}\boldsymbol{P})_{M_1}\prod_{M_2=1}^{N_{mu}}\det(\boldsymbol{U}^{-1}+\boldsymbol{T}^{sub}\boldsymbol{K}^{mu})_{M_2}\\&\times\prod_{M_3=1}^{N_{self}}\det[\boldsymbol{K}^{self}+(\boldsymbol{K}^{self}\boldsymbol{T}+\boldsymbol{E})\boldsymbol{P}]_{M_3}=0\end{aligned} \tag{28b}$$

where N_{point}, N_{mu} and N_{self} are the number of the point transmission, the mutual joint and the self joint, respectively, and where the symmetry of the $\boldsymbol{P}$, $\bar{\boldsymbol{T}}$ and $\boldsymbol{T}^{sub}$ are utilized. The final process of Eq. (28b), $\det(\boldsymbol{I}_{3n}+\bar{\boldsymbol{T}}\boldsymbol{P})_{N_{point}}$ or $\det(\boldsymbol{U}^{-1}+\boldsymbol{T}^{sub}\boldsymbol{K}^{mu})_{N_{mu}}$, corresponds to $G_1(\omega)$ or $G_2(\omega)$, respectively. The modified frequency equation (28b) has the following advantages:

(1) There is no classification for cases 1 and 2. Both cases are unified in Eq. (28b).

(2) The computation of each determinant in Eq. (28b) is accompanied with the transmission rules of Eqs. (13), (22), (25) and (26). There are no additional computational costs.

(3) Since the asymmetric poles are transformed into symmetric poles, only the plus or minus sign of $G(\omega)$ is treated in a simple implementation of the bisection method.

3.8 Characteristic mode

The procedure to obtain a characteristic mode is carried out in the reverse order to obtain the dynamic influence coefficient matrices. It starts from the right-hand side of the system and terminates with the left-hand side of the system. The dynamic influence coefficient matrices, which were already obtained, play a roll in obtaining a characteristic mode. Most of the process is common in cases 1 and 2 of **Fig. 9**, but the treatment of the initial point is differs in both cases. The initial treatment of each case is separately described as follows:

(*Case 1*) : After the final step of the computation of the dynamic influence coefficient matrix, Eq. (27a) is available under the condition of $\boldsymbol{f}'=\boldsymbol{0}$. Thus, the force vector $\{(\boldsymbol{f}_r^1)^{\mathrm{T}},\cdots,(\overline{\boldsymbol{f}}_r^i)^{\mathrm{T}},\cdots,(\boldsymbol{f}_r^n)^{\mathrm{T}}\}^{\mathrm{T}}\Rightarrow\overline{\boldsymbol{f}}$ is determined by Eq. (27a) with one fixed element, where all the right-hand ends of the main system are denoted node *r*. Substituting the determined $\overline{\boldsymbol{f}}$ into Eq. (16a) with all subscripts *r*, we obtain a displacement vector at the right-hand end of the system $\{(\boldsymbol{d}_r^1)^{\mathrm{T}},\cdots,(\boldsymbol{d}_r^i)^{\mathrm{T}},\cdots,(\boldsymbol{d}_r^n)^{\mathrm{T}}\}^{\mathrm{T}}\Rightarrow\boldsymbol{d}'$. After that, displacement vectors are recurrently obtained in the reverse order to obtain the dynamic influence coefficient matrices. In case 1, since the final route to compute the dynamic influence coefficient matrices was the *i*-th main system toward the node *r*, the displacement vectors $\boldsymbol{d}_{r-1}^i,\boldsymbol{d}_{r-2}^i,\cdots$ are computed by Eqs. (15a), (10) and (15b) with all subscript $j-1$ as:

$$\boldsymbol{f}_{j-1}^i=\boldsymbol{L}_j^i\overline{\boldsymbol{f}}_j^i,\quad \boldsymbol{d}=\boldsymbol{T}\boldsymbol{f},\quad \overline{\boldsymbol{f}}_{j-1}^i=\boldsymbol{f}_{j-1}^i-\boldsymbol{P}_{j-1}^i\boldsymbol{d}_{j-1}^i \tag{29a}$$

Recursive operation of Eq. (29a) with respect to $j=r,r-1,\cdots$ yields $\boldsymbol{d}_{r-1}^i,\boldsymbol{d}_{r-2}^i,\cdots$. Only the *i*-th block of $\boldsymbol{d}=\boldsymbol{T}\boldsymbol{f}$ is operated in order to save the computational costs. This operation continues until a mutual joint or branch point. For example, the operation continues until node *b* (branch point) in **Fig. 10**.

(*Case 2*) : The inner force vector from CE $\{\cdots,\{0_3\},-(\boldsymbol{f}_v^{CE})^{\mathrm{T}},\{0_3\},\cdots,\{0_3\},(\boldsymbol{f}_v^{CE})^{\mathrm{T}}\}^{\mathrm{T}}\Rightarrow\boldsymbol{f}^{CE}$ is determined by Eq. (27b) under the condition of $\boldsymbol{f}^{sub}=\boldsymbol{0}$, where one element of $-\boldsymbol{f}_v^{CE}$ or $\boldsymbol{f}_v^{CE}$ is fixed. Then, the displacement vector $\{(\boldsymbol{d}_r^1)^{\mathrm{T}},\cdots,(\boldsymbol{d}_r^i)^{\mathrm{T}},\cdots,(\boldsymbol{d}_r^n)^{\mathrm{T}},(\boldsymbol{d}_v^{sub})^{\mathrm{T}}\}^{\mathrm{T}}\Rightarrow\boldsymbol{d}^{sub}$ is obtained by Eq. (20), where all the right-hand ends of the main system are also denoted node *r*. Computation of the displacement vectors of subsystem $\boldsymbol{d}_{v-1}^{sub},\boldsymbol{d}_{v-2}^{sub},\cdots$ follows since the final route to compute the dynamic influence coefficient matrices was done in the subsystem. This process is implemented as same as in case 1.

$$\overline{\boldsymbol{f}}_j^{sub}=\boldsymbol{f}_j^{sub}-\boldsymbol{P}_j^{sub}\boldsymbol{d}_j^{sub},\quad \boldsymbol{f}_{j-1}^{sub}=\boldsymbol{L}_j^{sub}\overline{\boldsymbol{f}}_j^{sub},\quad \boldsymbol{d}=\boldsymbol{T}\boldsymbol{f} \tag{29b}$$

Recursive operation of Eq. (29b) with respect to $j=v,v-1,\cdots$ yields $\boldsymbol{d}_{v-1}^{sub},\boldsymbol{d}_{v-2}^{sub},\cdots$. This process also continues until node 0 of the subsystem.

Treatment of a branch point, a mutual joint and a process after both points are common to cases 1 and 2. An example of a branch point is node *b* in **Fig. 10**. The force vector $\boldsymbol{f}_b^i,\boldsymbol{f}_0^{sub}$ and

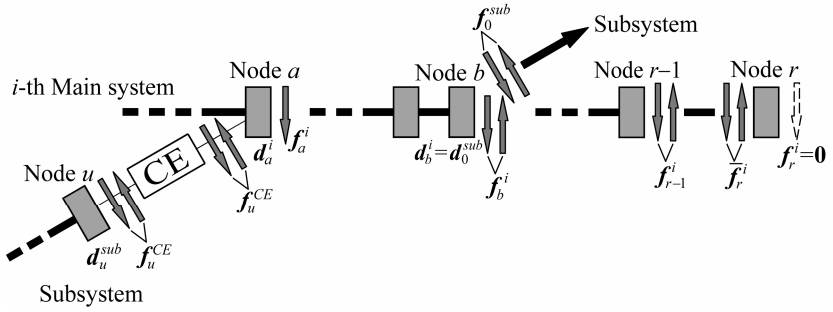

Fig. 10 Sample process to obtain a characteristic mode.

displacement vector $\boldsymbol{d}_b^i$ are known at node b after the operation of Eqs. (29a) and (29b). Computation of displacement vectors $\boldsymbol{d}_{b-1}^i, \boldsymbol{d}_{b-2}^i, \cdots$ from Eq. (29a) follows but the initial force vector is given as: $\overline{\boldsymbol{f}}_b^i = \boldsymbol{f}_b^i + \boldsymbol{f}_0^{sub} - \boldsymbol{P}_b^i \boldsymbol{d}_b^i$. This is because the force vector from the subsystem $\boldsymbol{f}_0^{sub}$ acts on node b in addition to $\boldsymbol{f}_b^i$.

An example of a mutual joint is node a in **Fig. 10**. The force vector $\boldsymbol{f}_a^i$ and displacement vector $\boldsymbol{d}_a^i$ are obtained by Eq. (29a) and the force vector $\boldsymbol{f}^{sub}$ of Eq. (27b) is known. The force vector $\boldsymbol{f}^{CE}$ is obtained from Eq. (27b). Following that, the subsystem connecting to node a in **Fig. 10** is similarly treated as the subsystem in **Fig. 9(b)**. The displacement vectors $\boldsymbol{d}_{u-1}^i, \boldsymbol{d}_{u-2}^i, \cdots$ are obtained from Eq. (29b) with respect to $j = u, u-1, \cdots$. Equation (29a) is still available to nodes $a-1, a-2, \cdots$ in **Fig. 10** but the initial force vector is given as: $\overline{\boldsymbol{f}}_a^i = \boldsymbol{f}_a^i - \boldsymbol{f}_u^{CE} - \boldsymbol{P}_a^i \boldsymbol{d}_a^i$. This is because the force vector from the CE $-\boldsymbol{f}_u^{CE}$ acts on node a in addition to $\boldsymbol{f}_a^i$.

If a self joint illustrated in **Fig. 8(a)** exists somewhere on the route, the relationship $\boldsymbol{f}_j^i = \overline{\boldsymbol{f}}_{j+1}^i$ is inserted into Eq. (29a) or Eq. (29b).

The process described above continues until it arrives at the left side ends of the main system. Finally, displacement vector of each node corresponds to a characteristic mode.

4. Numerical Computations

In order to demonstrate the feasibility of the newly presented algorithm of the TICM, numerical computations were implemented. A standard computer (CPU 1.0 GHz, 256 MB RAM) was used. The compiler was Fortran 95, and double precision variables were used unless in a special case. An ordinary determinant method, which is formulated as the following equation, was also implemented.

$$\det(\boldsymbol{K} - \omega^2 \boldsymbol{M}) = 0 \tag{30}$$

where $\boldsymbol{M}$ and $\boldsymbol{K}$ are the mass matrix and the stiffness matrix of the whole system. In this paper, we call this method Large Matrix Method (hereafter: LMM). The validity of the TICM is estimated by a comparison between the TICM and the LMM. We made several devices to accelerate the computational speed of the LMM as much as possible. For example, non-zero elements of $(\boldsymbol{K} - \omega^2 \boldsymbol{M})$ were gathered nearby the diagonal part, and computation of zero-elements was eliminated from the routine.

4.1 Analytical model

An analytical model is illustrated in **Fig. 11**. The system consists of n lines of horizontal main systems and vertical, slanting subsystems. Every joint in **Fig. 11** is modeled as a pin joint, in which

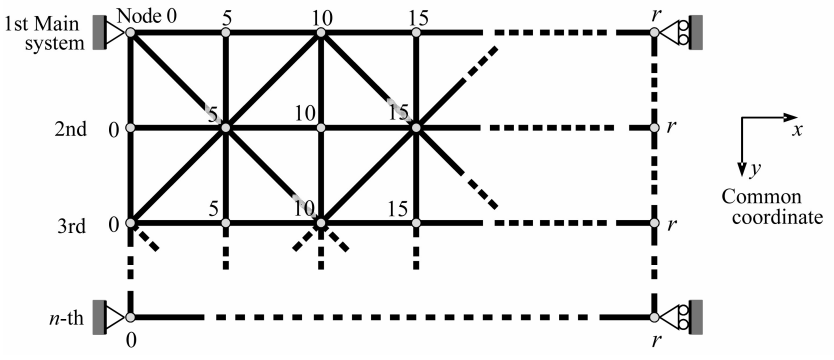

Fig. 11 Analytical model of an in-plane frame structure.

the spring constants of CE are given as $k_x^{CE}, k_y^{CE} \to \infty, K^{CE} = 0$. Hence, the analytical model is an in-plane truss structure. Simply supports exist at node 0 of the 1st and the *n*-th main systems. The supports are realized by $\hat{k}_{x,j}^i, \hat{k}_{y,j}^i \to \infty, \hat{K}_j^i = 0$, ($i = 1, n, j = 0$). Simply supports with sliding (vertical direction) exist at node *r* of the 1st and the *n*-th main systems, which are realized by $\hat{k}_{x,j}^i \to \infty, \hat{k}_{y,j}^i, \hat{K}_j^i = 0$, ($i = 1, n, j = r$). Practical values corresponding to infinity "∞" are specified later.

All the members of the system are solid steel shafts 20 mm in diameter. The length of each horizontal and vertical member sectioned by pin joints is 500 mm. The length of each slanting member is $500 \times \sqrt{2}$ mm. The horizontal, vertical and slanting members are equally divided into 5, 5 and 7 pieces, respectively, for the lumped mass modeling. The characteristic values of inertia (mass and moment of inertia) are equally separated into the both sides of the divided pieces.

The route of the computation to obtain the dynamic influence coefficient matrices ***T*** on this model is shown as a flowchart in **Fig. 12**. The maximum dimension of ***T*** is only 3(*n*+1) if the computation of ***T*** follows the route in **Fig. 12**.

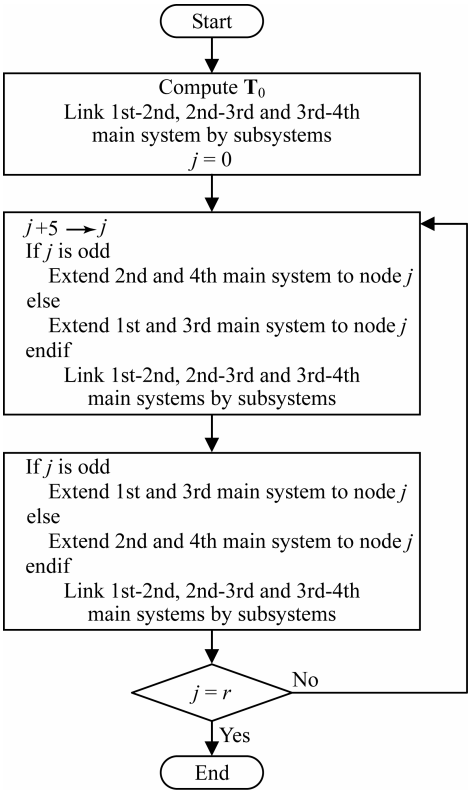

Fig. 12 Flowchart of a computation of the dynamic influence coefficient matrices.

The information of the analytical model, for example, length, diameter and slanting angle of the member, spring constants, the route of the computation of ***T***, etc., are specified in a parameter file. The actual computation of free vibration analysis follows an input process of the information into an executive file. If another analytical model is treated, only the parameter file is altered. No other executive file is needed for another analytical model. Many types of in-plane frame structures are treatable according to the parameter file. We emphasize that the source program of the TICM is general-purpose. As for the LMM, the same parameter file is utilized to arrange the mass matrix ***M*** and the stiffness matrix ***K***.

4.2 Computational accuracy

We treated an analytical model of $n=4$ and $r=35$ (**Fig. 11**). The degrees of freedom of the model was given by

$$N_{DOF}=3(n-1)(14r/5+6)+18nr/5 \tag{31}$$

$N_{DOF}=1440$ in this case. The frequency equation (28b) of the TICM and Eq. (30) of the LMM were solved by the bisection method. Frequency $f=\omega/(2\pi)$ (Hz) was used in place of the circular frequency ω (rad/s). The bisection method started from 0.1 Hz with an initial frequency step size 0.1 Hz. A natural frequency was obtained as f when the plus or minus sign of the frequency equation changed between f and $f+\Delta f$, and the frequency step size Δf satisfied $\Delta f/f<10^{-10}$.

Spring constants k_x^{CE}, k_y^{CE} and $\hat{k}_{x,j}^{i}, \hat{k}_{y,j}^{i}$ ($i=1,\ n,\ j=0$) were modeled as infinite in pin joint and simply support, respectively, while $\hat{k}_{y,j}^{i}$ ($i=1,\ n,\ j=r$) was infinite in the simply support with sliding. In a practical computation, finite large value was used as a substitution for infinite. In this paper, the LMM with quadruple precision variables was also implemented and spring constants $\hat{k}_{x,j}^{i}=\hat{k}_{y,j}^{i}=10^{20}$ N/m was chosen as a large value. The result of the LMM with quadruple precision was regarded as an exact solution of the truss structure. The natural frequency of quadruple precision was computed under the condition of $\Delta f/f<10^{-20}$ and the 1st natural frequency, about 67.3 Hz, was obtained. The spring constants in the TICM and the LMM of double precision were represented as 10^s N/m, where the parameter s ranged from 10 to 20. The 1st natural frequencies to the parameter s were computed by the TICM and the LMM of double precision. The relationship of the parameter s and relative errors of the 1st natural frequencies to the exact solution are plotted in **Fig. 13**. The results of the TICM uniformly converged at the exact solution. Since the solution of double precision was obtained under the condition of $\Delta f/f<10^{-10}$, the relative errors were almost saturated at 10^{-10}. As for the LMM of double precision, the results converge at the exact solution while s =10, ... ,15 but suddenly deviate from the exact solution as s becomes larger than 15. It is clear that the TICM kept the computational accuracy even if the spring constants became very large, but the LMM lost accuracy as the spring constants became large. The loss of accuracy in the LMM was caused by numerical instability due to the large values of the spring constants. Although the result of the LMM of double precision is possibly used in a practical use, it implicitly involves a numerical instability when a spring constant is very large. On the contrary, the TICM is quite free from such numerical instability.

Typical characteristic modes to the parameter $s=15$ are shown in **Fig.14**. Since the 2nd – 5th

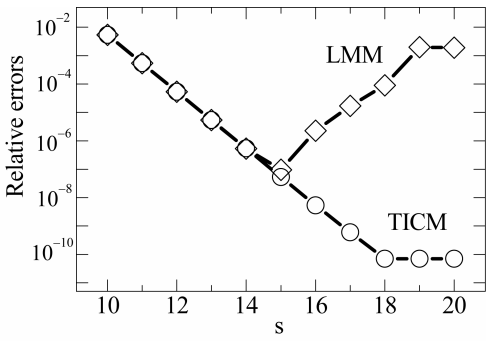

Fig. 13 Relative errors of the 1st natural frequencies of analytical model ($n=4$, $r=35$) with spring constant 10^s N/m ($s=10, 11, \ldots, 20$) to the exact 1st natural frequency (quadruple precision with spring constant 10^{20} N/m).

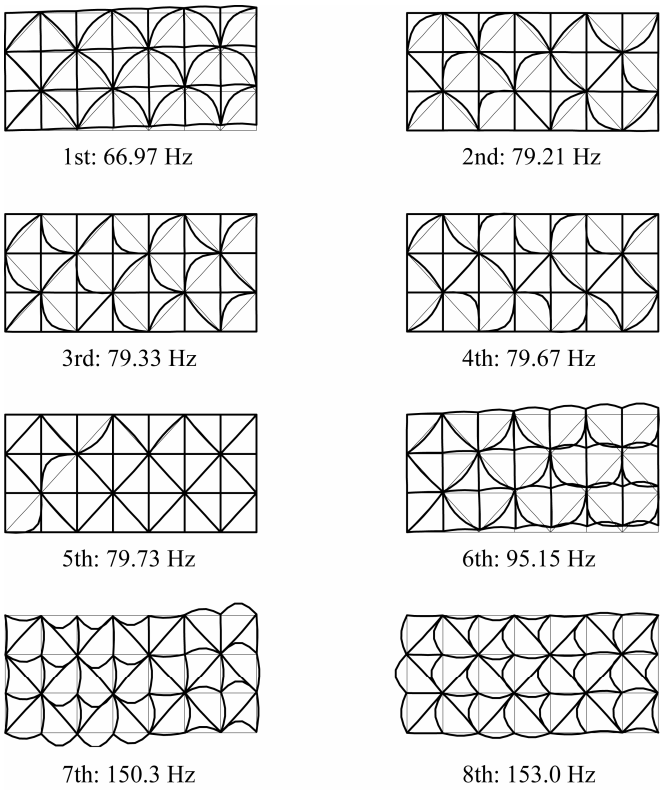

Fig. 14 Typical characteristic modes.

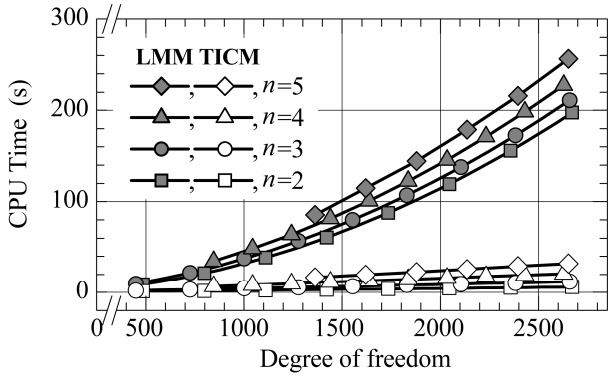

Fig. 15 Computational speed.

natural frequencies are close to each other, the shape of corresponding characteristic modes, in which only the slanting members are vibrating, are similar to each other.

4.3 Computational speed

The computational times of the TICM and the LMM are compared in this section. An analytical model was the same as in Section 4.2. The spring constant of 10^{10} N/m was selected in order to prevent numerical instability in the LMM. CPU times to operate the frequency equation [Eq. (28b) for the TICM, Eq. (30) for the LMM] 1000 times were provided for the comparison. The relationships between the CPU times and N_{DOF} are plotted in **Fig.15**, where the CPU times are

classified into numbers of the main system $n = 2$, 3, 4 and 5. The CPU times increase in both methods as N_{DOF} increases, but the TICM is wholly faster than the LMM. The computational time of the LMM increases at a higher rate than that of the TICM. Since the computational speed of the LMM needed to be accelerated to its maximum potential, the TICM has a distinct advantage in computation speed, especially in large scale structures.

The operation of the LMM was impossible in a range of $N_{DOF} > 2700$ on the employed computer, while the TICM was able to operate without such limitations. The limitation of the LMM is directly affected by N_{DOF} because the dimension of the matrix used in the LMM corresponds to N_{DOF}. On the contrary, the maximum size of the matrices and vectors in the TICM is only $3(n+1)$ according to the computational route shown in **Fig. 12**. It is clear that the TICM also has an advantage in computational storage.

5. Conclusions

(1) The algorithm of the Transfer Influence Coefficient Method was extended to an in-plane frame structure which includes branches and links to form closed loops. The newly extended algorithm enabled the free vibration analysis of truss and rahmen structures.

(2) Source program code according to the presented algorithm was able to treat various type of in-plane frame structure. No other program code was needed for different analytical models. Only a parameter file, which included information of the analytical model, was altered.

(3) The feasibility of the presented algorithm was demonstrated through some numerical computations. The presented algorithm had advantages in computational accuracy and speed compared with that of the ordinary determinant method.

Although the algorithm in this study was restricted within an in-plane free vibration of a two-dimensional frame structure in order to simplify the description, the algorithm will be easily extended to three-dimensional structure. Force vibration, transient response and nonlinear response are also treatable. That will be a future work.

References

1) D.C. Zimmerman, S.W. Smith, et al.; An Experimental Study of Structural Health Monitoring using Incomplete Measurements. ASME J. Vib. and Acoustics, Vol.118, pp.543-550 (1996).
2) C.R. Farrar and G.H. James III, System Identification from Ambient Vibration Measurements on a Bridge, J. Sound and Vib., Vol.205, pp.1-18 (1997).
3) J.L. Crassidis and D.J. Mook, Integrated Estimation/Identification Using Second-Order Dynamic Models, ASME J. Vib. and Acoustics, Vol.119, pp.1-8 (1996).
4) R.J. Guyan, Reduction of Stiffness and Mass Matrices, American Institute of Aeronautics and Astronautics Journal, Vol.3, p.380 (1965).
5) N. Bouhaddi and R. Fillod, Model Reduction by a Simplified Variant of Dynamic Condensation, J. Sound and Vib., Vol.191, pp.233-250 (1996).
6) A.Y.T. Leung, Dynamic Stiffness and Substructures, Springer-Verlag, Berlin, (1993).
7) N. Petersmann, Calculation of Eigenvalues Using Substructures and Dynamic Condensation, Proc. Np Int. Conf. on Recent Advances in Structural Dynamics, Southampton, UK, pp.211-219 (1984).
8) W.L. Qu, Z.H. Chen, et al.; Dynamic Analysis of Wind-Excited Truss Tower with Friction Dampers, Computers and Structures, Vol.79, pp.2817-2831 (2001).
9) H. Imai, C-B. Yun, et al., Fundamentals of System Identification in Structural Dynamics, Probabilistic Engineering Mechanics, Vol.4, pp.162-173 (1989).

10) E.C. Pestel and F.A. Leckie, Matrix Methods in Elastomechanics, McGraw-Hill Publishers, New York, (1963).
11) A. Sueoka, H. Tamura, et al., A Method of High Speed Structural Analysis Using a Personal Computer, Bulletin of JSME, Vol.28, pp.924-930 (1985).
12) T. Kondou, A. Sueoka, et al., Free Vibration Analysis of a Distributed Flexural Vibrational System by the Transfer Influence Coefficient Method, Theoretical and Applied Mechanics, Vol.37, pp.289-304 (1989).